Analysis of the Amorphous and Interphase Influence of Comonomer Loading on Polymer Properties towards Forwarding Bioadvantaged Copolyamides

Sanaz Abdolmohammadi,^{a,b,‡} Dustin Gansebom,^{a,b,‡} Shailja Goyal,^a Ting-Han Lee,^a Baker Kuehl,^a
Michael J. Forrester,^a Fang-Yi Lin,^a Nacú Hernández,^a Brent H. Shanks,^{a,b} Jean-Philippe

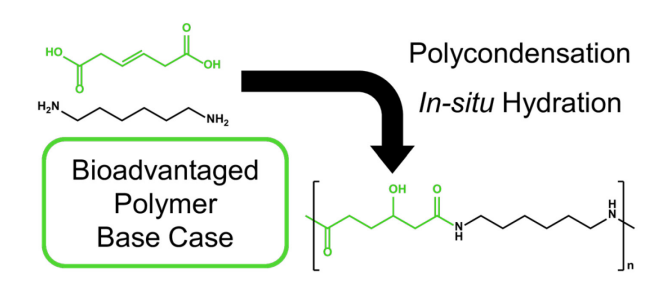
Tessonnier, *a,b Eric W. Cochran *a

^aDepartment of Chemical and Biological Engineering, Iowa State University, 618 Bissell Road, Ames, Iowa 50011, United States

^bCenter for Biorenewable Chemicals (CBiRC), 617 Bissell Road, Ames, Iowa 50011, United States

^{*} Corresponding authors

for Table of Contents use only



ABSTRACT Here we present an approach for selectively modifying the properties of semicrystalline polymers by introducing "bioadvantaged" counits. With this approach, the unique functionality of biomass can be leveraged to tailor the properties of the amorphous phase of semicrystalline polymers with minimal impact on crystallinity and thermomechanical properties. As a model case, PA 6,6 copolyamides were produced using the bioadvantaged monomer trans-3-hexenedioic acid (t3HDA). The analogous structure of t3HDA to adipic acid, a PA 6,6 monomer, allows for seamless integration. Screening over the entire composition range identified the t3HDA loading (20 mol%) beyond which properties deviate appreciably from Nylon 6,6. Once identified, copolyamides of suitable compositions were upgraded to commercial quality and fully characterized to assess the influence of counit loading and polymer structure on thermal and mechanical properties. Samples were characterized using gel permeation chromatography (GPC), proton nuclear magnetic resonance spectroscopy (¹H NMR), heteronuclear single quantum coherence spectroscopy (HSQC), wide-angle X-ray scattering (WAXS), differential scanning calorimetry (DSC), thermogravimetric analysis (TGA), dynamic mechanical analysis (DMA), tensile testing, flexural testing, and water absorption testing. t3HDA units were shown to hydrate during the harsh polycondensation to 3-hydroxyhexanedioic acid (3HHDA) and fully incorporate into the polymer backbone. Loading levels up to 20% were shown to have comparable thermal and mechanical properties in the dry state, yet moisture absorption—a known method for improving the toughness, yield strain, and elongation of polyamideswas enhanced by over 100% at 20% loading. This case study on bioadvantaged copolymers elucidates the governing structure-function principles that can be leveraged to forward value-added renewable polymers.

1 Introduction

The use of agricultural products and residues as feedstocks for chemicals has been pursued for many years as concerns over the sustainability of chemical manufacturing have grown increasingly prominent. However, despite extensive effort, widespread commercial adoption of biomass as a chemical feedstock has not materialized. Achieving a sustainable chemical industry necessitates a reassessment of the prevailing view that sustainability is the principal goal of biomass conversion technology. Many of the first such efforts focused on drop-in chemicals that directly compete with existing petrochemicals and fuels, including short and long chain fatty acids, phenolics, methane, and ethanol.¹⁻⁴ The Department of Energy has promoted this approach by releasing a list of the top value-added chemicals that can be derived from biomass. 5,6 The drop-in replacement approach, while appealing from a technical perspective as the markets and infrastructure for utilizing these products already exist, suffers from vulnerability to enduring price volatility in crude oil and natural gas. Consequently, interest in drop-in renewable fuels has historically vacillated with the price of oil.^{7,8} Over the past decade, unfavorable economics and low oil prices have led to the bankruptcy, closure, or liquidation of numerous biorenewables companies and plants. 9-13 In the long term, oil prices will continue to receive downward pressure from renewable energy adoption, making it increasingly difficult for the drop-in replacement approach to be economically viable. To enhance the adoption of biomass as a chemical feedstock, an alternative approach is required.

To create sustainable markets for biomass, it has been proposed to exploit its unique properties to yield novel chemicals that were previously inaccessible through crude oil.¹⁴ Novel biobased chemicals have untapped potential and no competition from the petrochemical industry. In contrast to drop-in chemicals,

capitalizing on the unique functionality of biomass to add value to petrochemical products has demonstrated efficacy. The prototypical example of this approach is furfural, which was serendipitously produced by the Quaker Oat company from oat hulls while attempting to enhance its digestibility as a cattle feed. At the time, no market existed for furfural, but by combining extensive experimentation and structure-function knowledge, applications in phenolic resins, refining, and usage as a solvent were established. 15,16 Furthermore, furfural was derivatized into other furanic compounds, broadening its usage. 16 Biobased furfural was integrated into the existing petrochemical industry as a complement, not as a substitute. The fact that furfural is still produced via biomass deconstruction nearly a century later is a testament to the tenacity of novel products derived from biomass. 15,17 Unfortunately, novel biobased chemical development faces technical barriers, despite its potential. Novel chemicals have no existing markets. As such, it is useful to identify an application beforehand to narrow the investigatory universe and guide research efforts. However, a dearth of structure-function knowledge encumbers rational design. Molecular targets cannot be identified, so a strictly retrosynthetic approach is inadequate. To overcome these challenges, a forward-synthetic approach based on "bioprivileged" molecules was recently described. Bioprivileged molecules are defined as "biology-derived chemical intermediates that can be efficiently converted to a diversity of chemical products including both novel molecules and drop-in replacements."14 The bioprivileged approach utilizes diversity-oriented synthesis to leverage the unique functionality of biomass and develop novel products. Furthermore, since they can be readily converted into drop-in chemicals, bioprivileged molecules can be viably produced regardless of market conditions by subsidizing the direct replacements with high value novel species. During periods of high demand, bioprivileged molecules can profitably be used to produce drop-in chemicals. The versatility of the bioprivileged approach keeps biomass conversion resilient in diverse economic conditions.

Another approach considered for advancing the adoption of biomass feedstocks is the "bioadvantaged" approach, which focuses on biomass valorization for polymer manufacturing. Bioadvantaged polymers are defined to offer unique performance advantages to their petrochemical counterparts by incorporating minimally modified biologically-produced monomers that are inaccessible to the petrochemical industry. 18 Unsaturated triglycerides, for example, have been extensively studied. Functionalization of the unsaturated bond with an epoxide and subsequent ring opening with alpha-beta unsaturated carboxylic acids such as acrylic acid and itaconic acid enabled the synthesis of thermosets, rubbers, styrenic block copolymers, and polylactic acid blends. 18-21 Polyols have received much attention as well. Renewable polyols have been used to produce hydrogels, polyurethanes, and polyesters.^{22–25} The unique functional combinations of these polymers offer the advantages necessary to encourage their adoption. For example, acrylated epoxidized soybean oil has been used to toughen polylactic acid, increase asphalt processability, and reduce asphalt thermal cracking.^{21,26} Polyol polyesters readily biodegrade and are biocompatible.²⁵ Without these advantages, there would be no impetus for assimilation into the preexisting chemical industry. Attempting to produce legacy polymers from biomass forces competition solely on price, leading to suppressed prices. Considering half of all shale oil wells are profitable below \$40/bbl, the minimum price required to cover operating expenses can be as low as \$10/bbl, and the largest expense for commodity chemical production is feedstock, it is challenging for biobased drop-in chemicals to compete economically.^{27–29} Developing polymers and chemicals that complement and enhance the established petrochemical portfolio is the best way to establish longstanding integration of biomass in the chemical industry.

The bioprivileged and bioadvantaged strategies complement each other, and combining them can further strengthen the value-driven adoption of biomass as a chemical feedstock. One molecule at the nexus of these approaches is muconic acid. Muconic acid is a C₆ alpha-gamma unsaturated diacid that can be

fermented from glucose and lignin by bacteria and yeast.^{30–34} Using chemical catalysis, muconic acid can be derivatized into numerous commodity chemicals currently derived from petroleum, including, adipic acid (AA), hexamethylenediamine (HMDA), caprolactone, caprolactam, and 1,6-hexanediol.³⁵ Muconic acid has also been derivatized into the novel species *trans*-3-hexanedioic acid (*t*3HDA) using an electrochemical process having 98% selectivity, 96% conversion, and nearly 100% faradaic efficiency.^{36,37} Technoeconomic analysis of this process suggested that *t*3HDA can be produced for \$2.13/kg.³⁷ Considering its appealing cost, *t*3HDA is a promising candidate for bioadvantaged polyamides. Furthermore, *t*3HDA's double bond can serve as a target for further functionalization. Grafting different functional moieties to *t*3HDA can lead to other bioadvantaged polymers with tailored properties. Prior to examining this potential, however, an assessment of the influence of counit loading on semicrystalline polymer properties is necessary.

Herein, we seek to demonstrate how the incorporation of bioadvantaged monomers in low loadings can lead to legacy semicrystalline polymers with value-added properties. By using low loadings, we postulate that a high degree of crystallinity can be maintained, thereby resulting in copolymers with comparable thermal and mechanical properties to their unloaded counterparts. Furthermore, we propose that the amorphous region is selectively altered by comonomer loading and that judicious selection of counit functionality can result in desirable properties. We have chosen Nylon 6,6 loaded with *t*3HDA as a model case for our approach due to the commercial relevance of Nylon 6,6 and the structural similarity of *t*3HDA to adipic acid, a Nylon 6,6 monomer. We first set out to screen these "bioadvantaged nylons" (BANs) over the entire composition range to identify the critical loading level where BAN properties begin to deviate significantly from those of Nylon 6,6. While BANs with higher loading levels doubtlessly have unique properties and applications worth examining further, they are beyond the scope of this work. Those

BANs with acceptable properties were upgraded to commercial quality and fully characterized to assess the influence of counit loading on crystalline structure, thermal properties, and mechanical properties.

2 Materials and Methods

2.1 Materials

AA and HMDA [98% purity], were purchased form Sigma Aldrich. *t*3HDA [>98% purity] was purchased from TCI America.

2.2 Monomer salt preparation

Prior to polymerization, t3HDA, AA and HMDA were prepared into HMDA-t3HDA and HMDA-AA salts to ensure proper end group stoichiometry. HMDA-t3HDA and HMDA-AA salts were prepared separately instead of producing a HMDA-AA-t3HDA salt in a single process to prevent composition drift due to possible differences in solubility. Salts were prepared by first dissolving AA and t3HDA separately in methanol (CH3OH). The resulting solutions were then separately mixed with solutions of HMDA in CH3OH such that the molar ratio of carboxylic acid units to amine units was 1:1. Each combined solution was then heated in a round bottom flask at 60 °C for at least 30 min. The precipitated salts were subsequently filtered, washed with CH3OH, and left to dry in a fume hood. The purity of each salt was verified using proton nuclear magnetic resonance (¹H NMR) spectroscopy and Fourier transform infrared (FTIR) spectroscopy. ¹H NMR spectra were collected using a Bruker Avance III 600 nuclear magnetic resonance spectrometer, and salts were dissolved in deuterium oxide for analysis. FTIR spectra were collected using a Thermo Scientific Nicolet iS5 FTIR spectrometer fitted with an iD7 ATR accessory. After drying, these salts were combined such that a target mole percentage of x diacid monomers were t3HDA.

2.3 Polymerization

BANs were prepared using a bulk polycondensation method. HMDA-AA-t3HDA salts with different amounts of t3HDA were polymerized in an autoclave reactor equipped with a heating jacket and an external temperature controller. The salt was mixed with 20-25 v/w% water prior to the reaction to facilitate adequate mixing. The reactor was then purged with nitrogen and pressurized to 150 psig to prevent oxidation and thermal decomposition. The first stage of the polymerization reaction consisted of stirring the wet salt at 150 rpm while the reactor was heated using a fixed set point of 265 °C for 2 h such that it reached an internal pressure of roughly 300 psig. Previous calibration showed that this set point yielded an internal temperature of roughly 230 °C. During the second stage of the polymerization, the reactor was then vented to atmospheric pressure and the polymer melt was stirred at 400 rpm while the reactor was heated at a set point of 300 °C for 2 hours. Previous calibration showed that this set point yielded an internal temperature of roughly 275 °C. After the second stage, the reactor was cooled, and the solid polymer was collected. Two batches of each BAN were made to produce sufficient sample for characterization. BANs were ground into a powder using a Retsch CryoMill, like batches were uniformly mixed, and BAN powders were dried at 80 °C under static vacuum for 48 h prior to processing and analysis. When appropriate, the abbreviation BANx will be used to indicate a BAN sample where x mole percent of the diacid units are novel monomer. For example, BAN0 has 0% t3HDA and is equivalent to unmodified Nylon 6,6.

2.4 Gel permeation chromatography

The molecular weight distribution of each BAN was characterized via gel permeation chromatography (GPC). GPC was carried out on BAN samples using a Tosoh Ecosec HLC-8320GPC equipped with a Tosoh TSKgel SuperAWM-H 150 x 6.0 mm column in series with two Agilent PL HFIPgel 250 x 4.6 mm columns along with RI and UV detectors. The solvent 1,1,1,3,3,3-hexafluoroisopropanol (HFIP) was used as the eluent, and sodium trifluoroacetate with a concentration of 0.02 mol/L HFIP was used as an additive

to prevent sample aggregation. Each sample had an injection volume of 10 μL and was analyzed at 45 °C under a 0.3 mL/min flow rate. The molecular weight of each BAN was calculated using a calibration curve based on Agilent PMMA standards. Considering the hydrodynamic volume of PMMA may not be similar to Nylon 6,6, molecular weights calculated using this standard method are likely inaccurate. To compensate for differences in hydrodynamic volume in the absence of suitable Mark-Houwink parameters, an empirical relationship similar in principle to the universal calibration method was also used. Briefly, Nylon 6,6 standards of known molecular weight were analyzed and their molecular weights were calculated using the aforementioned PMMA calibration curve to create a map linking the hydrodynamic volumes and associated molecular weights of PMMA and Nylon 6,6. Molecular weights determined using this method will be said to be in terms of Nylon 6,6, while molecular weight calculated from the PMMA calibration curve will be said to be in terms of PMMA. To form this map, Nylon 6,6 standards purchased from American Polymer Standards were used. The molecular weight of each Nylon 6,6 standard was first calculated using the PMMA calibration curve. The resulting Nylon 6,6 molecular weights in terms of PMMA were then plotted against American Polymer Standards' reported values. Curve-fitting was used to develop a relationship between molecular weight in terms of PMMA and molecular weight in terms of Nylon 6,6. Using this curve-fitting function, the molecular weight of BANs were determined in terms of Nylon 6,6. Additional details are provided in Section A of the ESI. For transparency, the results of both methods are provided.

2.5 Nuclear magnetic resonance spectroscopy

A Bruker Avance III 600 nuclear magnetic resonance spectrometer was used to collect ¹H NMR spectra of each BAN. To dissolve BANs, a solution of two parts trifluoroacetic anhydride and one part deuterated chloroform was used. Tetramethyl silane (TMS), included at 1 v/v% in the deuterated chloroform, was used as reference. The spectrum of BAN0 was subtracted from the other spectra to isolate new peaks

attributable to *t*3HDA loading. To quantify the inclusion of novel monomer into the polymer, the ratio of novel monomer to the total number of repeat units was calculated using proton integrations:

$$r_{obs} = \frac{I_{1H}}{(I_{tot}/22)}$$

where r_{obs} is the observed ratio, I_{IH} is the integration of a single proton attributed to the novel monomer, I_{tot} is the total integration of all polyamide signals, and 22 is number of protons in a repeat unit. To assess novel monomer inclusion, the resulting ratios were compared to expected values based on the degree of t3HDA loading:

$$r_{exp} = X_{t3HDA}$$

where r_{exp} is the expected proton ratio for complete incorporation and X_{t3HDA} is the mol fraction of t3HDA loaded.

A Bruker NEO 400 nuclear magnetic resonance spectrometer was used to collect heteronuclear single quantum coherence (HSQC) spectra of each BAN. Samples were dissolved in the same solvent system used for ¹H NMR (*vide supra*). Samples were heated to 40 °C and spun at 20 Hz to reduce sample viscosity and minimize convection. The number of scans was 256. Using BAN0 as a reference, novel cross peaks were used to identify methylene hydrogens, methine hydrogens, and hydrogens not bound to a carbon atom.

2.6 Wide-angle X-ray scattering (WAXS)

Temperature-dependent wide-angle X-ray scattering (WAXS) measurements were performed using a XENOCS Xeuss 2.0 SWAXS system with monochromatized light of wavelength $\lambda = 0.7107$ Å from Mo K α radiation. Data were collected using a silver behenate-calibrated Pilatus 1M detector at a sample-to-detector distance of 33.97 cm. The corresponding scattering vector (q) window for this setup is 0.1-3.5 Å. Annealed (*vide infra* Section 2.8), powdered samples were sealed in aluminum hermetic pans and fixed to a temperature controlled Linkam THMS600 stage equipped with an LNP95 liquid nitrogen cooling

pump. Data was acquired in 10, 15, or 20 °C intervals from room temperature up to within 10 °C of the melting point determined via differential scanning calorimetry. Both heating and cooling sweep data were collected to observe potential hysteresis. Each sample was equilibrated at the desired temperature for 10 min followed by a 10 min acquisition. The percent crystallinities of annealed samples were calculated by integrating the (100), (010/110), and (002) reflections and normalizing them to the total pattern integral, including the amorphous halo. Prior to integration, diffractograms were scaled and the aluminum pan signal was subtracted. Integration was facilitated by fitting the diffraction pattern to four gaussians with a quadratic baseline. All diffractograms were smoothed using a 5-point adjacent average smoothing protocol to improve clarity.

2.7 Thermal properties

Thermal studies were performed using thermogravimetric analysis (TGA), differential scanning calorimetry (DSC), and dynamic mechanical analysis (DMA). TGA measurements were carried out using a NETZSCH STA model STA 449 F1 Jupiter thermogravimetric analyzer. Each TGA sample weighing 3-5 mg was analyzed in an alumina crucible pan from 80 to 700 °C with a heating rate of 10 °C/min under nitrogen atmosphere with a flow rate of 10 mL/min. DSC was conducted on polymer powder sealed in hermetic aluminum pans using a TA Instruments DSC. A typical DSC temperature program consisted of cycling the sample over an appropriate temperature range to observe all thermal transitions at a heating/cooling rate of 10 °C/min under nitrogen atmosphere with a flow rate of 50 mL/min. Samples were cycled through heating and cooling twice to establish a consistent thermal history prior to cycling a third time for analysis. DMA was performed using a TA instrument ARES-G2 rheometer with a 3-point bending fixture under nitrogen gas flow to prevent thermal degradation. All samples were injection molded into 64 x 12.7 x 3.2 mm Izod bars using a HAAKE MiniJet Pro and annealed (*vide infra* Section 2.8). Samples were analyzed continuously from -30 to the 175 °C at a heating rate of 5 °C/min, a flexural

strain of 0.05%, and a frequency of 1 Hz to determine the glass transition temperature, storage modulus at 30 °C, and loss modulus at 30 °C.

2.8 Mechanical properties

The mechanical properties of BANs were determined using tensile and flexural tests. Mechanical test specimens were prepared using a HAAKE MiniJet Pro for injection molding. Prior to molding, specimens were powdered and dried (*vide supra* Section 2.3) to minimize hydrolytic degradation. After molding, specimens were annealed at approximately 200 °C under dynamic vacuum for 48 h to ensure all samples had a common thermal history. Injection molded samples were then stored in a desiccator and/or parafilm sealed containers to minimize ambient moisture absorption between tests. Tensile test specimens were prepared according to standard ISO 527-2 1BB. Tensile properties were measured using a 3369 series Instron Universal Testing Machine with a 10 mm/min extension rate. Multiple tensile bars were tested for statistics, and outliers were excluded to obtain data sets of 7 to 10 specimens per sample. Specimens were excluded as outliers if they failed prior yield, shortly after yield, or after inordinate necking. Flexural test specimens were molded into 64 x 12.7 x 3.2 mm Izod bars. Flexural tests were carried out according to standard ASTM D790 using a 3369 series Instron Universal Testing Machine equipped with a 3-point bend fixture. Briefly, 3 mm thick samples were subject to a 0.01 mm/mm/min strain rate using a support span of 50 mm.

2.9 Moisture absorption

Moisture absorption measurements were carried out at room temperature (25 °C) on unannealed 64 x 12.7 x 3.2 mm Izod bars. Triplicate specimens of each sample were analyzed for statistics. All specimens were dried at 80 °C for 48 h under static vacuum prior to being massed on a Mettler Toledo XS105 microbalance with \pm 0.01 mg precision. Each specimen was then immersed in 18.2 M Ω DI water for 12 days to approximate the equilibrium water absorption. Unabsorbed water was wiped off the surface of the

specimens after removing them from the water, then the mass of each specimen was quickly measured using the microbalance.

Moisture absorption was calculated using the following equation

$$A = \left[\frac{W - D}{D}\right] \times 100$$

where A is the moisture absorption (%), W is the mass of the wet specimen (g), and D is the mass of the dried specimen (g).

3 Results and discussion

BANs were synthesized by loading biobased *t*3HDA into Nylon 6,6 as a comonomer to assess the influence of counit loading on structural, thermal, and mechanical properties. These results are summarized in Tables 1, 2, and 3, respectively.

Table 1. BAN structural properties with different *t*3HDA loadings.

Sample	$M_n^a (kDa) (fA/gB)$	$ \Theta^{b}(kDa)(^{f}A/^{g}B) $	r _{exp} ^c	$r_{obs}{}^d$	Dev ^e (%)
Commercial PA66	57.1/— ^h	2.14/— ^h	_	_	
BAN0	30.0/17.1	1.96/2.01		_	
BAN5	29.7/16.7	1.97/2.04	0.05	0.0459	8.2
BAN10	28.6/16.3	1.95/2.04	0.10	0.1073	7.3
BAN20	28.2/16.2	1.95/2.03	0.20	0.2132	6.6

^aNumber average molecular weight (M_n). ^bDispersity (Đ). ^cExpected proton ratio (r_{exp}). ^dObserved proton ratio (r_{obs}). ^eDeviation between r_{exp} and r_{obs} (Dev). ^fWhere A is in terms of PMMA. ^gWhere B is in terms of Nylon 6,6. ^hResults are invalid due to extrapolation beyond the calibration limits.

Table 2. BAN thermal properties with different t3HDA loadings.

Sample	$T_g^a (^{\circ}C)$ T_m^b $(^{\circ}C)$	T _c ^c (°C)	$\Delta H_c^d (J/g)$	DSC χ _c ^e (%)	 T ₅ ^g (°C)	Res ₅₀₀ ^h (%)

Commercial PA66	79.3	260.0	233.8	47.0	30.9	_	409.4	4.4
BAN0	79.3	257.1	223.9	43.6	19.3	72.2	394.2	3.8
BAN5	78.2	253.6	219.3	42.2	18.7	71.4	393.6	6.6
BAN10	74.5	247.0	211.3	38.7	17.1	69.0	391.8	6.6
BAN20	72.3	233.4	192.1	32.1	14.2	67.2	395.0	6.9

^aGlass transition temperature determined using DMA (T_g). ^bMelting temperature (T_m). ^cCrystallization temperature (T_c). ^dEnthalpy of crystallization (ΔH_c). ^ePercent crystallinity from DSC (DSC χ_c). ^fAnnealed sample percent crystallinity from WAXS (WAXS χ_c). ^gDecomposition temperature at 5% mass loss (T_5). ^hResidual mass at 500 °C (Res₅₀₀).

Table 3. BAN physical properties with different *t*3HDA loadings.

Sample	E"a (MPa)	E'b (GPa)	E ^c (GPa)	TS ^d (MPa)	TT ^e (MPa)	UE ^f (%)	F ^g (GPa)	FS ^h (MPa)	H ₂ O Abs ⁱ (%)
Commercial PA66	64	2.93	1.13 ± 0.03	98 ± 4	70 ± 17	80 ± 20	2.8 ± 0.5	127 ± 6	3.94 ± 0.06
BAN0	70	2.85	1.13 ± 0.03	98 ± 5	49 ± 7	57 ± 8	3.2 ± 0.1	131.2 ± 0.6	3.46 ± 0.09
BAN5	71	3.08	1.14 ± 0.01	99 ± 3	44 ± 2	51 ± 2	3.3 ± 0.1	135 ± 1	4.30 ± 0.04
BAN10	92	3.15	1.23 ± 0.05	105 ± 5	52 ± 5	56 ± 6	3.5 ± 0.1	142 ± 1	5.269 ± 0.007
BAN20	74	3.43	1.20 ± 0.03	102 ± 8	49 ± 16	59 ± 18	3.6 ± 0.1	148 ± 2	8.8 ± 0.3

^aLoss modulus at 30 °C (E"). ^bStorage modulus at 30 °C (E'). ^cTensile modulus (E). ^dTensile strength (TS). ^eTensile toughness (TT). ^fUltimate elongation (UE). ^gFlexural modulus (F). ^hFlexural strength (FS). ⁱMoisture absorption (H₂O Abs).

GPC results showed that BANs were synthesized with similar molecular weights and low dispersity, thus eliminating the influence of molecular weight on polymer properties from consideration. *t*3HDA was shown to hydrate to 3-hydroxyhexanedioic acid (3HHDA) *in situ* and to fully incorporate into the polymer

backbone using ¹H NMR and HSQC. The proposed reaction is outlined in Scheme 1. Thermal properties, including glass transition temperature (T_g), melting temperature (T_m), crystallization temperature (T_c), and crystallization enthalpy (ΔH_c), were found to decrease with increased t3HDA loading. Using DSC and WAXS, percent crystallinity (χ_c) was found to decrease as well. Similar absolute χ_c reductions were observed regardless of crystal growth via melt cooling (DSC) or annealing (WAXS). A second order transitions was observed with DSC for BANs with higher t3HDA loading. The heat capacity change during this transition increased with t3HDA loading, providing evidence of a hydrogen bond network in the amorphous phase due to the 3HHDA hydroxyl group. Interestingly, the elasticity as measured by the storage modulus (E') increased with t3HDA at low temperatures before reversing trend at higher temperatures. These observations can also be attributed to the 3HHDA hydroxyl group. Said hydroxyl group reduces packing efficiency, thereby increasing the free volume of the amorphous region at elevated temperatures above which the denser hydrogen bond network disintegrates. Reduced packing efficiency also prevents counit inclusion in crystal lamellae, resulting in reduced crystallinity on account of statistical limitations to crystal growth. Mechanical properties testing, however, indicated that χ_c reduction was only minor for the loading levels examined. Tensile and flexural testing showed that the t3HDA loading had minor or insignificant effects on mechanical properties, which is expected considering the mechanical properties of semicrystalline polymers are largely dependent on crystallinity. Thermal and mechanical tests were conducted on dry samples, however, and these properties are known to be impacted by moisture absorption. Considering this influence, moisture absorption tests were performed and it was found that t3HDA loading increases moisture absorption. This observation is easily explained by the hydroxyl group of 3HHDA, which is not only hydrophilic but also reduces crystallinity via packing disruption. The enhanced hydrophilicity of BAN could make it well suited for applications that require high levels of conditioning. Nylons are typically conditioned to enhance toughness, yield strain, and elongation at break.

It is conceivable that BANs could be used, for example, in performance athletic fabrics, since flexibility and moisture management are highly desirable properties in this market. BANs' reduced melting point could also ease processing by reducing the energy costs associated with melt processing and injection molding.

Scheme 1. *In-situ* Hydration of *t*3HDA during Polymerization

$$H_2$$
N H_2 H_3 O H_4 H_5 O H_5 H_7 O H_7 H_8 H_8

The BANs previously discussed (*vide supra*) were chosen for in-depth analysis based on their similar properties to Nylon 6,6. To identify which *t*3HDA compositions gave similar properties, screening was conducted over the entire composition range.

3.1 Compositional screening of bioadvantaged nylons (BANs)

To determine which BAN compositions were suitable as Nylon 6,6 alternatives, BANs across the entire composition spectrum were screened. To facilitate facile synthesis and screening, samples were generated using a tube furnace polymerization, which resulted in lower molecular weights. Sample preparation and characterization methods are provided in Section B of the ESI.

The thermal properties of these BANs are summarized in Section C of the ESI. Screening results showed that increasing *t*3HDA loading decreased the melting point (T_m). T_m continued to decrease up to 50% *t*3HDA loading, beyond which no melting transition was observed. Similarly, the crystallization temperature (T_c) decreased until the copolymer became completely amorphous. Increasing *t*3HDA loading decreased the glass transition temperature by up to 60 °C (17%) at 100% loading. Using dynamic mechanical analysis (DMA), the storage modulus at 30 °C was observed to decrease with increased loading. In contrast, the loss modulus was observed to steadily increase up to 50% loading, beyond which it dropped rapidly.

X-ray diffraction (XRD) and WAXS results are summarized in Section D of the ESI. XRD experiments showed a drop in crystallinity (χ_c) up to 50% t3HDA loading, at which point the copolymers became completely amorphous. This is with the exception of BAN5, which had slightly higher crystallinity than BAN0. Temperature dependent WAXS studies showed that t3HDA loading increased the Brill transition temperature at low loadings, but ultimately suppressed it at higher loadings because of the reduced melting temperature of BANs with high t3HDA loading. An in-depth description of the Brill transition temperature is provided in Section 3.4.

Based on the screening results, it was found that BAN properties begin to significantly deviate from those of Nylon 6,6 above 20% t3HDA loading. Since BAN must be similar to Nylon 6,6 for it to be a suitable alternative, BANs with 20% or less t3HDA were chosen to be upgraded to commercial quality. The resulting high molecular weight samples were fully characterized using structural, thermal, and mechanical analyses.

3.2 Molecular weight determination

The GPC chromatograms obtained for independent batches of each BAN sample are shown in Figure 1. The results indicate that the polymerization process was reproducible. Based on the chromatograms, all samples have similar peak molecular weights and peak widths.

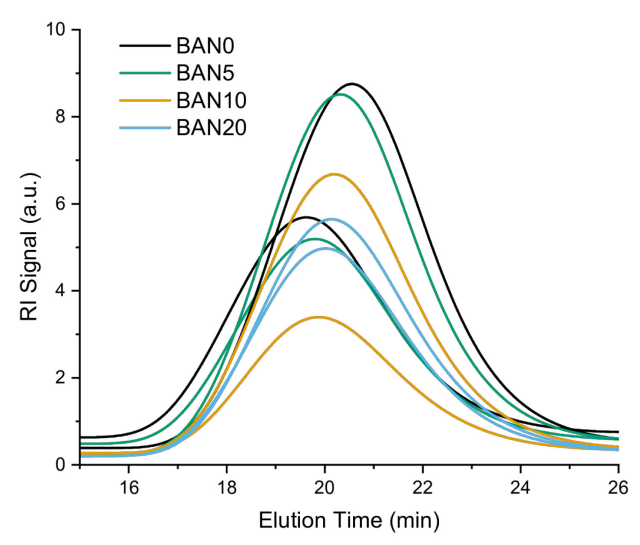


Figure 1. Gel permeation chromatograms of BANs with different *t*3HDA loadings. Samples were made in two batches and analyzed separately.

Molecular weights in terms of both PMMA and Nylon 6,6 (vide supra Section 2.3) further corroborate these results. The molecular weights of all BANs are within 1 kDa of each other. Furthermore, number average molecular weights in terms of Nylon 6,6 are greater than 15 kg/mol, and dispersities are approximately 2. This indicates that the BANs produced in this study are of commercial quality. Commercial quality Nylon 6,6 typically has a number average molecular weight between 15 and 30 kg/mol. For comparison, Nylon 6,6 purchased from Sigma Aldrich (Commercial PA66) was also analyzed. The molecular weight of Commercial PA66 was found to be about twice that of BAN samples. The lower molecular weight of BAN samples is attributed to non-optimized polymerization conditions. H NMR and FTIR spectra indicate that BAN salts were pure prior to polymerization, ensuring that chain ends were not prematurely capped, thus limiting molecular weight. BAN salt H NMR and FTIR spectra are provided in Section E of the ESI. Despite BAN samples having sufficiently high molecular weights to be classified as commercial grade, it is worthwhile to compare them to a commercial sample of higher molecular weight. It is well known that the molecular weight of polymers has a significant effect on their properties up to a limiting molecular weight, so it is necessary to ensure that molecular weight is

sufficiently high for unambiguous comparisons to be made with commercial Nylons.^{38,39} While polymerization conditions were not sufficiently optimized to produce samples with molecular weights comparable to Commercial PA66, the results discussed in the next sections (*vide infra*) indicate that the molecular weight is sufficiently high for thermal and mechanical properties to not change with further increase. To rationalize how *t*3HDA loading influences polymer properties, the chemical structure of BAN was determined.

3.3 Chemical structure determination

The chemical structure of BAN was analyzed using ¹H NMR and HSQC. BAN spectra are shown in Figure 2. The peaks labeled PA are characteristic of Nylon 6,6 and correspond to the methylene protons of condensed adipic acid and hexamethylene diamine. As the *t*3HDA loading increased, 8 distinct signals appeared and gradually increased in intensity. These novel peaks are marked with * in Figure 2. The chemical shifts of these peaks were inconsistent with the 2 alkene and methylene signals that would be expected of *t*3HDA loading. Furthermore, no signal was observed in the 5-6 ppm region characteristic of disubstituted, unconjugated alkenes. This suggests *t*3HDA reacted during the harsh reaction conditions of the polycondensation process.

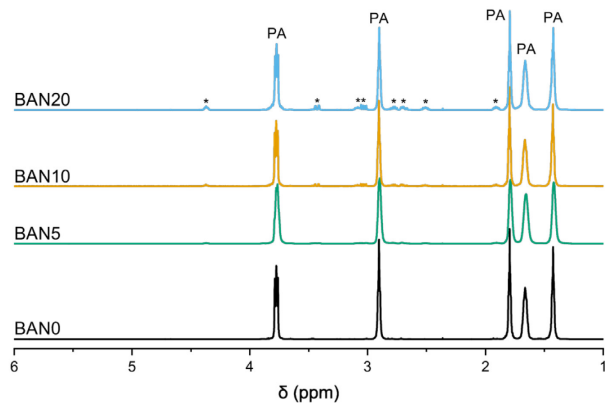


Figure 2. ¹H NMR spectra of BAN0 (black), BAN5 (green), BAN10 (orange), and BAN20 (blue). Peaks characteristic of Nylon 6,6 are marked with PA, and peaks attributed to *t*3HDA loading are marked with

To identify the new repeat unit produced during the reaction, the observed number of new signals, chemical shifts, relative integrations, and couplings were all considered. New signals attributable to the novel monomer were isolated by subtracting out the BAN0 spectrum. This removed all characteristic Nylon 6,6 signals, including end group signals which overlapped with the signals of interest. A representative fully analyzed spectrum of BAN20 is shown in Figure 3 along with the proposed structure. Peak 2 has a 4.37 ppm chemical shift, suggesting that it is geminal to an electronegative moiety such as a hydroxyl group. Integration revealed that each novel peak had a relative integration of 1, implying that each peak corresponds to a single proton. Analyzing *J*-couplings showed that the number of coupling partners for each proton is largely consistent with the proposed structure, but complex multiplet patterns precluded a complete analysis. Furthermore, clear second order coupling was observed for peak pairs 1 and 4, suggesting they correspond to geminal hydrogens. *J*-couplings between peak 2 and peak pair 1 are notably consistent with a hexagonal chair conformation, which is likely favored due to hydrogen bonding between the proposed hydroxyl group and the proximal carbonyl group.

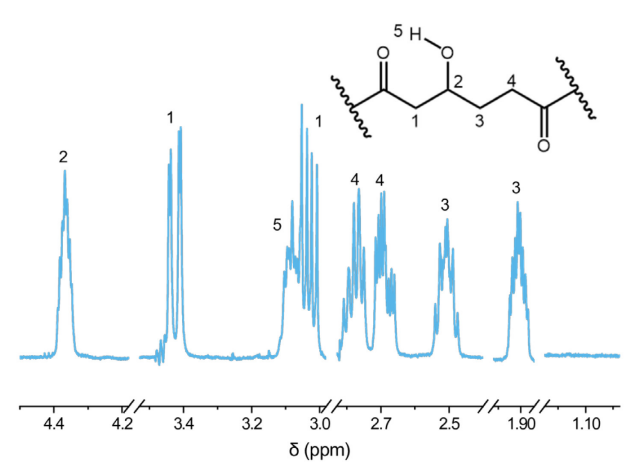


Figure 3. Magnified spectrum showing the novel BAN20 signals and the proposed structure. Overlapping end group signals were subtracted out. Numbers correspond to tentative proton assignments. The spectrum was taken in a solution of 66 v/v% trifluoroacetic anhydride and 33 v/v% CDCl₃ with tetramethylsilane (TMS) as an internal standard. 1 H NMR (600 MHz) δ 4.37 (tt, J = 8.1, 3.7 Hz, 1H), 3.43 (dd, J = 17.6, 3.6

Hz, 1H), 3.11 - 3.06 (m, 1H), 3.03 (dd, J = 17.6, 9.3 Hz, 1H), 2.78 (dt, J = 17.6, 8.6 Hz, 1H), 2.69 (ddd, J = 17.9, 10.0, 5.1 Hz, 1H), 2.56 - 2.45 (m, 1H), 1.91 (ddt, J = 13.8, 9.3, 4.6 Hz, 1H).

HSQC was used to corroborate the structural conclusions drawn from ¹H NMR. A representative overlay of BAN0 and BAN10 HSQC spectra is shown in Figure 4. Additional HSQC spectra showing phases are provided in Section F of the ESI. Novel ¹H NMR peaks were found to correspond to novel ¹³C peaks, though in some cases these peaks overlapped with other, stronger peaks and could not be observed. Cross peaks 1, 3, and 4 were found to correspond to methylene groups, while cross peak 2 was found to correspond to a methine group. Notably, peak 5 had no corresponding cross peak in the HSQC spectra, showing that, as anticipated, it is not bound to a carbon atom. The ¹³C shift of cross peak 2 is within the characteristic range of COH carbons, further corroborating *in-situ* hydration and the proposed structure. While two additional cross peaks were observed that do not correspond to 3HHDA, these peaks are attributable to HMDA proximal to 3HHDA in the polymer chain.

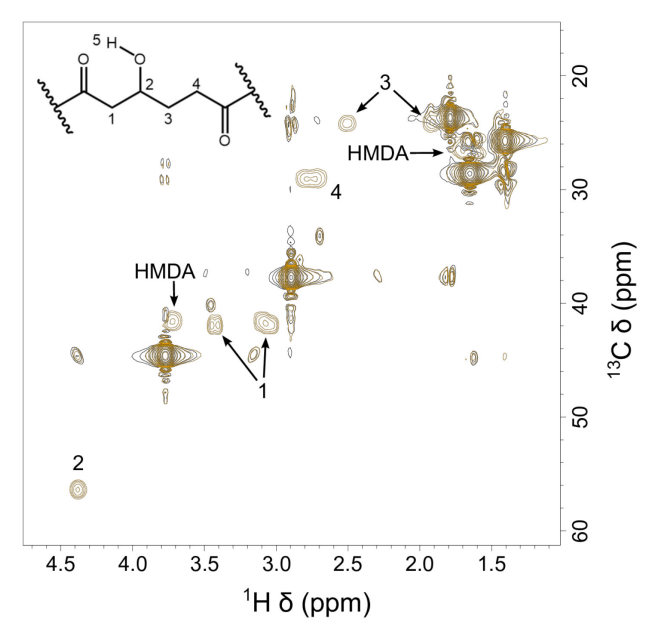


Figure 4. Overlaid HSQC spectra of BAN0 (black) and BAN10 (orange). Cross peaks corresponding to HMDA proximal to 3HHDA are labeled.

¹H NMR and HSQC data support the conclusion that *t*3HDA is hydrated to 3HHDA during the polymerization process. The addition of water as a mass transfer promoter as well as the high-temperature and high-pressure conditions are believed to drive the hydration reaction. The observations that no new signals were produced other than those of 3HHDA and that all samples were solubilized in HFIP without difficulty suggest that any branching or crosslinking due to esterification reactions between the 3HHDA hydroxyl group and other diacids is minimal, if present at all. The continual production of water during the condensation reaction and ready hydrolysis of esters when exposed to pressurized steam⁴⁰ likely prevents the formation of branched or crosslinked products. Although it might be predicted that any hydroxyl group would react with the trifluoroacetic anhydride solvent, reactions between sterically hindered alcohols and anhydrides often require catalysts for the reaction to proceed.^{41–43} Despite the revelation of a change in structure during the polymerization reaction, *t*3HDA will continue to be identified as the loaded monomer for simplicity. Reference will be made to 3HHDA when appropriate.

To substantiate the complete incorporation of *t*3HDA into the polymer, ¹H NMR integration ratios were examined. Excellent agreement was observed between experimental and expected results, which deviated by less than 10%. Considering the relatively small signal-to-noise ratio of the novel signals, the possible exacerbation of noise due to the spectral subtraction process, and the presence of both positive and negative deviations which is characteristic of random error, we conclude that *t*3HDA was fully incorporated into the polymer. Full inclusion would be expected to influence crystallization behavior, so we set out to elucidate the influence of *t*3HDA loading on crystal structure.

3.4 Crystalline structure determination

To evaluate the effects of comonomer loading on crystallization and crystalline structure, temperature dependent WAXS experiments were conducted. Room temperature (25 °C) WAXS patterns are shown in Figure 5. Two peaks characteristic of Nylon 6,6 are clearly observed at 2θ angles of approximately 9.3

and 11.0°, corresponding to the (100) and (010/110) doublet reflections of the triclinic α-phase, respectively. ^{44,45} A weak (002) reflection at about 6.2° 2θ was also observed, which has been reported by others as well. 46,47 The intrasheet (100) reflection is due to scattering within the polymer chains of a single polymer sheet, and the intersheet (010/110) reflection is due to scattering between different polymer sheets connected by hydrogen bonds. 45,46,48 The d spacing and relative intensities of the (100) and (010/110) reflections are unaffected by t3HDA loading, suggesting the comonomer is completely excluded from the crystal lattice. Complete exclusion of comonomer units from the crystal lattice has been observed in studies on other semicrystalline polymers as well. 49 In cases where counits are excluded from the crystal lattice, it is well established that the counit loading hinders crystallization by retarding the lamellar structure. 50-53 However, given sufficient time and provided that the comonomer loading is low, chain migration above the glass transition temperature enables well-developed crystals to form. 50,53 Furthermore, counits are expelled from crystals and accumulate on the crystal surface.⁵⁴ In the case of t3HDA loading, the thermodynamic preference for crystallization is sufficiently high for the degree of crystallinity to be minimally affected up to 20% loading. χ_c decreased monotonically from 72.2% to 67.2% as t3HDA loading increased.

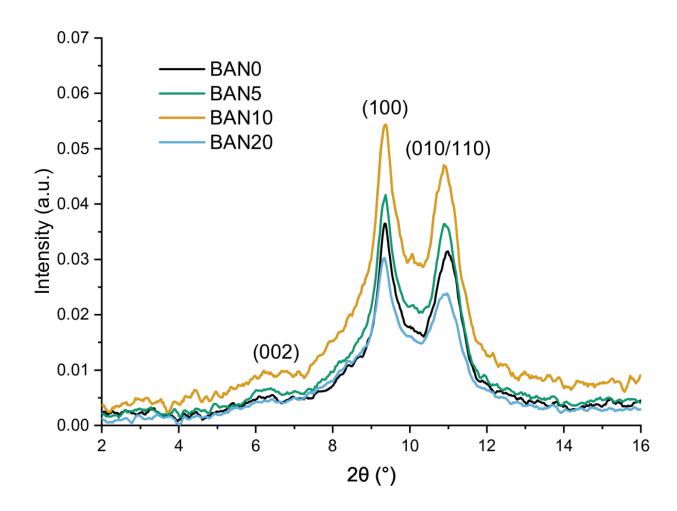


Figure 5. Wide angle X-ray scattering diffractograms of BANs at room temperature (25 °C) showing the intrasheet (100) reflection and the intersheet (010/110) doublet. Diffractograms have been smoothed for clarity.

Three dimensional WAXS temperature scans and corresponding d spacing plots are shown in Figure 6. Nylon 6,6 and polyamides in general undergo a crystal phase transition, the eponymous Brill transition, at elevated temperatures. During this transition, the interchain (100) peak and the intersheet (010/110) peak shift to higher and lower scattering vectors (q), respectively, until they merge at a specific temperature called the Brill transition temperature (T_b). 45-48 The merging of these peaks is attributed to the transition of denser triclinic crystals to a less dense pseudohexagonal or, alternatively, secondary triclinic structure. 45,47,55 Though the nature of the Brill transition is still debated 45, studies have shown that it is highly dependent on processing conditions, crystal structure, and morphology. 44,45,47 The T_b of Nylon 6,6 has been observed to vary from 139 °C to 230 °C depending on processing conditions, which is commonly rationalized as the result of variations in crystal perfection and lamellar thickness. 44,45 WAXS and SAXS experiments on Nylon 10,10 showed that T_b increases with increasing lamellar thickness.⁵⁶ Our temperature-dependent WAXS experiments showed that T_b decreased monotonically with increasing t3HDA loading. This suggests that t3HDA loading reduces lamellar thickness and that the chains adopt at least a partially random microstructure. Considering all comonomer units are excluded from crystals, lamellar thickness must be restricted by the statistical number of contiguous crystallizable units in a chain segment. 50,53 A wholly block microstructure would not significantly restrict the lamellar thickness beyond its natural upper bound, so it must be concluded that BAN microstructure is partially if not wholly random. Notably, T_b on cooling was higher for BAN10 and BAN20 than T_b on heating. A previous temperaturedependent WAXS study demonstrated hysteresis by varying the isothermal crystallization temperature and attributed the hysteresis to variations in crystal perfection.⁴⁴ It might be proposed that the increased

T_b on cooling, then, can be attributed to lamellar thickening. However, this interpretation cannot fully explain the results observed in this study. Samples were annealed to maximum crystallinity prior to analysis and were not heated above the melting temperature during WAXS. No hysteresis was observed for BAN0 and BAN5, further indicating that no additional lamellar thickening was possible. Postulating that lamellar thickening occurred during the duration of the experiment is untenable and must be dismissed. Hence, an alternative explanation is required.

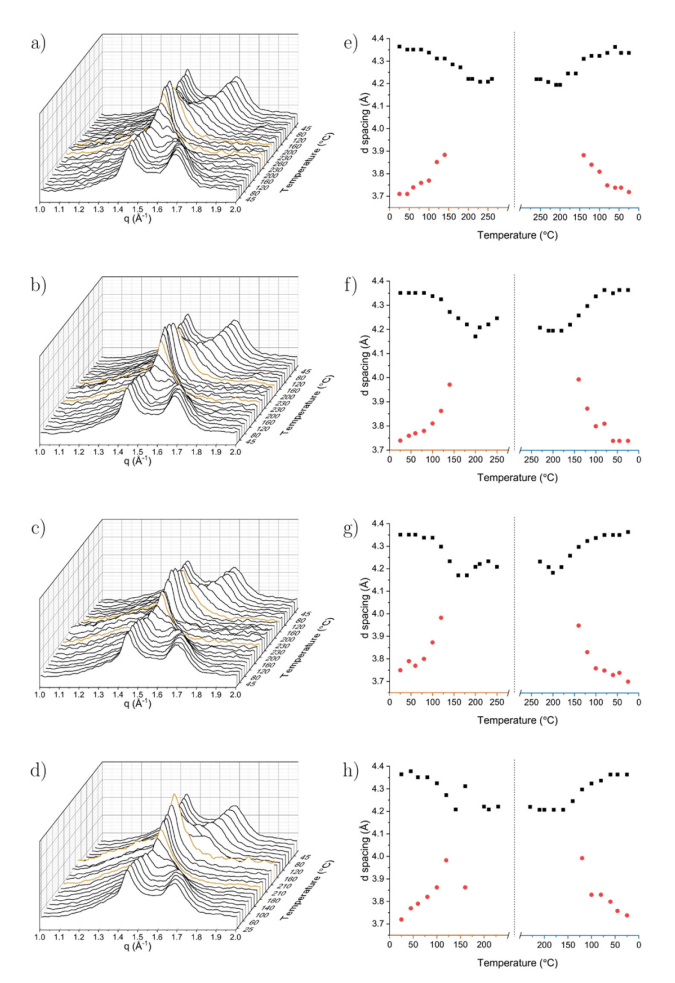


Figure 6. Three-dimensional temperature dependent WAXS patterns for (a) BAN0, (b) BAN5, (c) BAN10, and (d) BAN20. Samples were cycled through heating (back) and cooling (front). Orange traces indicate the Brill transition temperature. (e-h) Respective plots for BANs exhibiting (100) (black squares) and (010/110) (red circles) *d* spacings through heating (left) and cooling (right).

We propose that the amorphous fraction surrounding crystallites influences the onset of crystal phase transitions, which has also been proposed by others.⁵⁷ To rationalize this, a brief explanation of polymer crystal morphology is warranted. Extensive evidence has shown that polymer crystals are comprised of lamellar chain stacks wherein the individual lamellae are often separate chains. In this model, crystal basal planes are populated with amorphous chain moieties that are anchored to the crystal via partial-chain inclusion in the lamellae. 58 Such moieties include dangling-ends, which extend into the amorphous bulk; loops, which double back into the crystal and form new lamellae; and tie chains, which span and connect different lamellar stacks.^{58,59} These dangling-ends and loops have been termed the rigged amorphous fraction (RAF) by some researchers due to their restricted mobility resulting from anchoring to crystal lamellae. Restricted mobility is said to increase the glass transition temperature (Tg) of the RAF. 54,59,60 It has been demonstrated that counit loading leads to RAF thickening relative to the crystal thickness when counits are completely excluded from the crystal lamellae. 49,54,61 This is presumed to be the result of counit accumulation in the RAF at the basal plane of the crystal surface and in the remaining mobile amorphous fraction (MAF). 49,54 It has also been observed that comonomer loading increases the surface energy at the crystal-RAF interface.⁶² Regarding the Brill transition, SAXS experiments have demonstrated simultaneous changes in the RAF.⁵⁵ Other researchers have noted the correlation between T_b and T_g in WAXS studies of transcrystalline Nylon 6,6.45 Based on the foregoing evidence, it is reasonable to conclude that t3HDA loading reduces the Brill transition temperature on heating by increasing interfacial surface energy between crystals and the RAF. The t3HDA-abundant RAF is believed to adopt a strained conformation while cooling, thus increasing the interfacial energy. This explains why the Brill transition on heating is lower than that on cooling for BANs with higher t3HDA loading. On heating, the RAF transitions from a high-energy strained conformation to a relaxed conformation above the Tg of the RAF. On cooling, however, the RAF is initially in an unstrained conformation and the thermodynamic influence

of the surface energy is less pronounced. Considering that t3HDA loading and temperature influence the interactions between the amorphous and crystalline phases, thermal properties experiments were conducted.

3.5 Thermal properties characterization

Using DSC, the relationship between crystalline and thermal effects were examined. DSC traces are plotted in Figure 7 to emphasize the influence of t3HDA loading on peak shape. T_m, T_c, and χ_c were observed to decrease with increased t3HDA loading. This agrees with preliminary screening results discussed previously (vide supra). Furthermore, T_m reduction supports the conclusion from the WAXS study that t3HDA loading reduces lamellar thickness. These results are attributed to the disruptive effect of comonomer inclusion on crystallization. Comonomer inclusion in polyamides retards crystallization by disrupting inter-lamellar hydrogen bonding. Upon further t3HDA loading increase, crystal formation becomes critically hindered such that BAN is completely amorphous at greater than 50% t3HDA loading. In addition to reduced intensity, T_m and T_c peak broadening was also observed with increased t3HDA loading. Melting range broadening has been observed in copolyesters and other copolyamides as well.^{51,52} This too can be attributed to reduced lamellar thickness provided the microstructure is random. ^{50,53} For comparison, Commercial PA66 was also analyzed using DSC. In contrast, T_m, T_c, and χ_c were all significantly higher than those of BAN0. This difference is presumed to be the result of small molecule additives that act as crystal nucleation sites. Nucleation sites can significantly increase crystal formation kinetics.⁶³

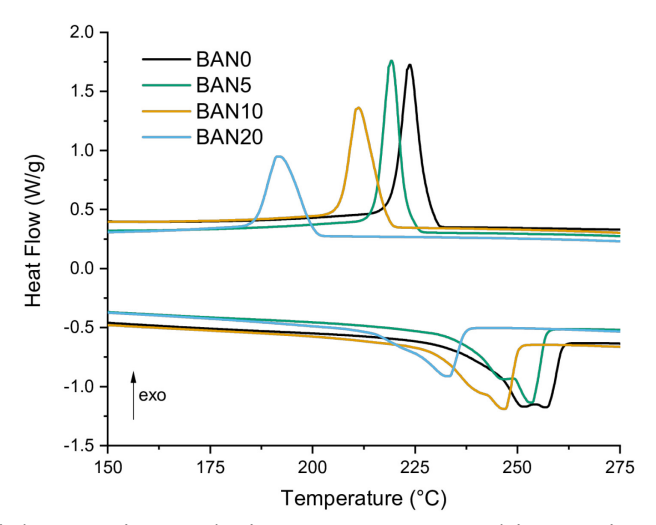


Figure 7. BAN differential scanning calorimetry traces. Melting point (T_m) and crystallization temperature (T_c) decrease and peak breadth increases as *t*3HDA loading is increased.

Considering the supporting evidence for *t*3HDA hydration and full exclusion of 3HHDA from the crystal lattice, a hydrogen bonded network in the amorphous fraction of BAN is anticipated. Such a network could be identified as a second order phase transition in DSC, since the disintegration of this network should cause a sharp change in heat capacity. As the degree of hydrogen bonding in the network increases, the magnitude of the heat capacity change should also increase. The low temperature region of each DSC trace was analyzed in Figure 8 to examine this possibility. Meeting expectations, a second order phase transition near 60 °C became increasingly pronounced with increased *t*3HDA loading.

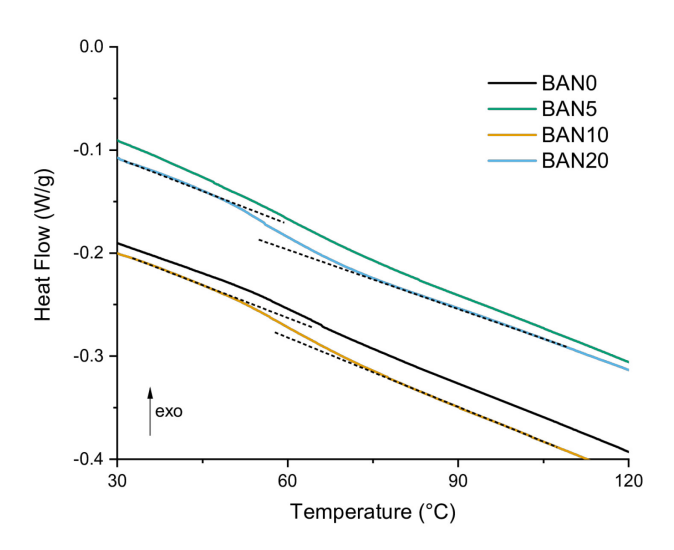


Figure 8. BAN differential scanning calorimetry traces revealing evidence of a second order phase transition attributed to a hydrogen bonding network. Exemplary dashed lines are provided to clarify the transition, which becomes more pronounced with increasing *t*3HDA loading.

Thermogravimetric analysis was performed on Commercial PA66 and BANs to investigate the influence of *t*3HDA loading on thermal stability and flame retardancy. Thermogravimetric curves are provided in Section G of the ESI. To assess measurement reproducibility, Commercial PA66 was analyzed 5 consecutive times. Thermogravimetric analysis indicated that Commercial PA66 and BANs of all compositions have the same decomposition temperature range between 320 and 500 °C.³⁹ The addition of *t*3HDA into the Nylon 6,6 system increased the residual mass at 500 °C by more than 50%. This suggests that BAN has some degree of intrinsic flame retardancy since char residue has been shown to correlate well with other flammability metrics when gas phase flame retardancy mechanisms are excluded.⁶⁴ Interestingly, the residual mass was independent of *t*3HDA loading for loadings between 5% and 20%. No consistent trend in the temperature at 5% mass loss (T₅) was observed when increasing *t*3HDA loading. For all loading levels examined, effects were minimal and less than 3 °C. Notably, T₅ was 15 °C lower for BAN0 compared to Commercial PA66. This can be attributed to the lower molecular weight and hence higher end group density of BAN samples, since thermal degradation in nylons is known to occur in part via chain end mechanisms.⁶⁵

Dynamic mechanical analysis was used to further examine the influence of t3HDA loading on the amorphous phase and its influence on properties relative to the crystalline phase. E', loss modulus (E"), and T_g were determined using this method. The E', E", and T_g values of Commercial PA66 and BAN0 were found to be nearly identical, as would be expected if BAN0 had sufficiently high molecular weight. E' and tan δ are plotted as a function of temperature for each BAN composition in Figure 9. E' measures a polymer's elasticity, while tan δ describes a polymer's damping ability. At lower temperatures, E' is

observed to increase with t3HDA loading, but this trend reverses above 68 °C. At lower temperatures, the 3HHDA hydroxyl group increases hydrogen bonding in the MAF and RAF, consequently increasing elasticity as measured by E'. Enhanced amorphous-fraction hydrogen bonding would be expected to decrease amorphous-fraction free volume, thereby increasing the viscous character of the polymer as measured by E".66 Matching expectations, E" was observed to increase with t3HDA loading when measured at 30 °C, though only slightly and well within experimental error. It is probable that the reduced packing efficiency afforded by comonomer loading largely counteracts the attractive force of hydrogen bonding. At higher temperatures, sufficient energy is provided for the amorphous hydrogen bonded network to be broken. The disintegration of said hydrogen bonding network causes elasticity to drop precipitously with increasing temperature, and this phenomenon becomes more pronounced with increased t3HDA loading. Enhanced t3HDA loading is thought to increase the degree of hydrogen bonding in the amorphous region, so this relationship is expected. After the amorphous hydrogen bonding network is broken and polymer chains can move freely, the effects of reduced packing efficiency dominate. The reduced packing efficiency increases free volume, so a decrease in Tg is expected. Using the peak of the tan δ curve, T_g was found to decrease with increasing t3HDA loading, matching expectations. To further examine the relative influences of the amorphous and crystalline phases on polymer properties, mechanical properties were examined.

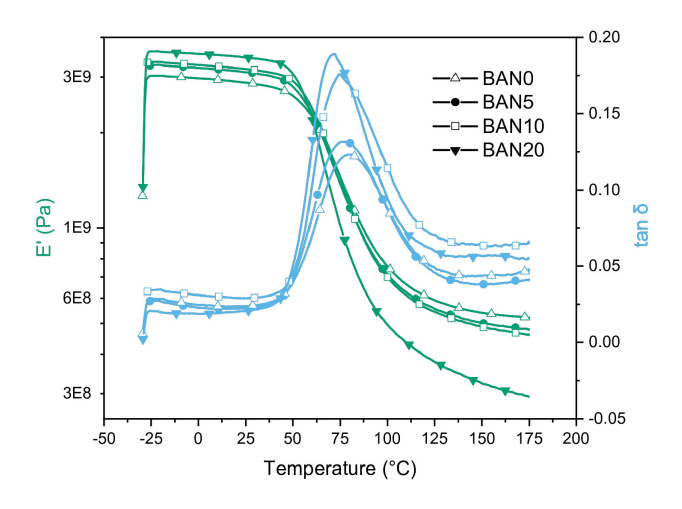


Figure 9. Dynamic mechanical analysis traces for BANs with different t3HDA loadings.

3.6 Mechanical properties testing

Tensile testing is one of the most common assessments of mechanical properties for engineering thermoplastics such as Nylon 6,6. Using an Instron Universal Testing Machine, the tensile modulus, tensile toughness, maximum stress, and maximum strain of annealed BANs were determined. Tensile stress versus strain plots and bar charts of derived quantities are available in Section H of the ESI. Notably, strain hardening is increasingly suppressed with t3HDA loading. Strain hardening has been attributed to the recrystallization of chains perpendicular to the strain axis following strain-induced melting.⁶⁷ This observation can therefore be attributed to t3HDA's suppressive influence on crystallization, which is affirmed by WAXS and DSC experiments. To verify that the molecular weight was sufficiently high for the mechanical properties to be independent of molecular weight, BAN0 was compared to Commercial PA66. The tensile modulus and maximum strain of BAN0 and Commercial PA66 are identical. While the average toughness and maximum strain of BAN0 and Commercial PA66 deviate by nearly 30%, it should be noted that these differences are statistically insignificant. All tensile properties except for the tensile modulus were observed to be statistically identical across the different BAN compositions studied. The tensile modulus of BAN10 and BAN20 were notably higher than BAN0 and BAN5, however only slightly. The observed mechanical property invariance is likely due to low loading and the similar chemical structure of the comonomer loaded. As observed in the WAXS experiments, t3HDA loadings less than 20% do not severely impair crystallization. The mechanical contribution of the crystalline domain is therefore similar for the compositions examined. Since 3HHDA, hydrated t3HDA, is structurally similar to adipic acid, it has a minimal effect on the mechanical properties of the amorphous domain that can only be observed in the tensile modulus at higher loadings. The toughness, maximum stress, and maximum strain remain unaffected. The larger tensile moduli of BANs with higher loadings

are likely due to a greater degree of hydrogen bonding afforded by the hydroxyl group of 3HHDA. Others have reported a similar result when studying the influence of hydrogen bonds in polymer networks.⁶⁸ The RAF, which in general is more rigid than the MAF, likely contributed as well.

Flexural testing is another common method for evaluating mechanical properties. To determine flexural property data, a 3-point bend apparatus was used. Flexural stress versus strain plots and bar charts of derived quantities are available in Section I of the ESI. In agreement with tensile data, flexural strain hardening was suppressed by *t*3HDA loading as well. This is likewise attributed to *t*3HDA's ability to hinder crystallization. Data collected include flexural modulus and flexural strength. For ductile polymers that yield and do not break during flexural testing, flexural strength is defined as the flexural stress at 5% strain.^{69,70} The high uncertainty associated with Commercial PA66 is due to an outlier to the downside that could not be justifiably excluded due to the limited number of specimens examined. However, regardless of exclusion or not, the flexural modulus and flexural strength of BAN0 and Commercial PA66 are identical within uncertainty. On average, both flexural modulus and flexural strength increased steadily with *t*3HDA loading. This further demonstrates the ability of 3HHDA to enhance amorphous region stiffness via increased hydrogen bonding and, more speculatively, RAF enhancement.

As previously noted, all mechanical property testing was performed on dry, annealed samples. Considering the extent of annealing—that is, the degree of crystallinity—and moisture content will undoubtedly influence mechanical properties, the trends observed in these tensile and flexural studies cannot easily be extrapolated to other conditions. While an exhaustive study of the multitude of possible processing scenarios is beyond the scope of this work, further insight can be achieved by simply assessing moisture absorption, which has a known influence on polyamide properties.

3.7 Moisture absorption testing

Due to the existence of hydrogen bonding amide linkages in the polymer chain, polyamides easily absorb water. Absorbed water molecules act as plasticizers, which change the dimensional stability of the polymer by reducing electrostatic interchain attraction. Furthermore, moisture absorption directly affects the physical and mechanical properties of polyamides.^{71–73} In the dry state, polyamides have enhanced modulus, strength, and abrasion resistance, but reduced toughness and flexibility. To enhance toughness, yield strain, and elongation at break, polyamides are often allowed to absorb moisture in a process called conditioning, though this is done at the expense of modulus, strength, and abrasion resistance.^{74,75} In engineering applications such as automotive parts, high strength and dimensional stability are desirable, so polyamides with reduced moisture absorption are preferred. In contrast, the flexibility of polyamides are highly desirable in the textile market, particularly in performance athletic wear. Biobased athletic fabrics are in demand and enjoy considerable growth.⁷⁶ There is therefore a strong demand for the ability to tailor polyamide properties to suit specific end-use applications, preferably with drop-in applicability.

To assess the moisture absorption of BANs, unannealed Izod bars were soaked in 18 M Ω water for 12 days to approximate equilibrium moisture content. Bar charts displaying the moisture absorption of Commercial PA66 and BANs of differing t3HDA loading are provided in Section J of the ESI. While the moisture absorption of BAN0 is statistically lower than Commercial PA66, this difference is not intrinsic to the polymer chemistry. Rather, the discrepancy is attributed to differences in crystallinity afforded by differing injection molding conditions and possibly additives. Depending on the polyamide molded, differing injection molding conditions were used to optimize melt flow and minimize thermal degradation. It is well known that processing parameters such as melt temperature, mold temperature, and injection pressure have a significant effect on polymer properties, especially the crystallinity of semicrystalline polymers. Reducing the crystallinity of polyamides is known to increase moisture absorption. While DSC experiments showed that Commercial PA66 has a higher crystallinity than in-house synthesized

BAN0, this observation need not hold true under different thermal conditions. DSC and WAXS studies showed that *t*3HDA loading decreased crystallinity. The reduced crystallinity imparted by *t*3HDA loading combined with the inherent hydrophilicity of the 3HHDA hydroxyl group can markedly increase water absorption. While the effects of processing conditions cannot be ruled out, a clear trend is observed as *t*3HDA loading increases. The results of this work suggest that processing conditions such as conditioning or annealing can be used to tailor the properties of BANs. Conditioned BANs may offer superior toughness and elongation at the expense of modulus and strength, while annealed BANs may offer sustainable polyamides with comparable properties to Nylon 6,6.

3.8 Takeaways and guidance

Considering many of the aforementioned conclusions regarding 3HHDA influence on polymer properties are not strictly linked to counit chemical structure but rather the result of loading level, it is reasonable to postulate that these results can be generalized to any randomly dispersed analogous counit. Such counits could include linear and cyclic difunctional monomers with any number of nonreactive pendent groups. It can be expected that trends observed in this study will be similar for most counit structures as a result of the dominating influence of crystallinity on polymer properties. While the crystal phase is unaffected by noncrystallizable counit loading level, the amorphous phase is more amenable to the unique structure of the counit. The 3HHDA hydroxyl group increased moisture absorption. It is conceivable that other functional groups could impart other properties. Recalling the bioprivileged concept, t3HDA could be used as a platform molecule to develop counits with novel functionality. For example, the t3HDA double bond could be used as a functional handle to graft on a hydrophobic alkyl chain, thereby decreasing nylon moisture absorption. To the same end, differing percentages of sebacic acid could be added to the Nylon 6,6 system, since this bioadvantaged monomer has been proven to reduce moisture absorption in Nylon 6,10.79 Using different percentages of hydrophobic monomer can allow for

moisture absorption and mechanical properties to be tailored to the application. Other functional advantages such as flame retardancy are also possible. We intend to examine this potential in future works. By using t3HDA as a platform, it is possible to develop a multitude of bioadvantaged products that add value to the petrochemical industry.

4 Conclusion

BANs of differing composition were synthesized as a model case for assessing the impact of comonomer loading on polymer properties. During batch polymerization, in-situ t3HDA hydration to 3HHDA was observed. Comonomers were found to partition into the amorphous and interphases while leaving the crystal phase unaltered. Increasing comonomer content minimally decreased χ_c up to 20% loading. In contrast, the dynamics of the amorphous and interphases were more significantly affected. Viscoelastic properties were observed to have an increased dependence on temperature with increased loading, attributed to the hydroxyl group influence of 3HHDA on hydrogen bonding and free volume. Moisture absorption, which occurs more readily through the amorphous phase, was found to increase by more than 100% at 20% loading. However, due to the dominating influence of crystallinity, thermal and physical properties were minimally affected up to 20% loading. These results suggest that bioadvantaged comonomers can be used to selectively alter polymer properties, namely those closely related to the amorphous and interphases. Furthermore, the structure-function relationship between comonomer loading and thermomechanical properties outlined in this study can be generalized to guide research on other randomly dispersed comonomers. By utilizing bioadvantaged monomers, value can be added to established polymer products. This approach which combines bioadvantaged and bioprivileged strategies uses added value to provide the impetus for biorefinery adoption while simultaneously minimizing capital requirements for product startup. Further development and implementation of this approach will aid the development of sustainable chemical industries.

AUTHOR INFORMATION

Corresponding Authors

*ecochran@iastate.edu *tesso@iastate.edu

Author Contributions

‡Sanaz Abdolmohammadi and Dustin Gansebom contributed equally. Shailja Goyal performed DMA and tensile testing experiments. Ting-Han Lee performed WAXS experiments and assisted with injection molding. Baker Kuehl assisted with WAXS experiments. Michael J. Forrester, Fang-Yi Lin, and Nacú Hernández assisted with experimental design.

Funding Sources

This material is based upon work supported in part by the National Science Foundation under the grant numbers IIP-1701000 and DMR-1626315 and the U.S. Department of Energy under grant number DE-EE0008492.

ABBREVIATIONS

t3HDA, trans-3-hexenedioic acid; BAN, bioadvantaged nylon; GPC, gel permeation chromatography;

¹H NMR, proton nuclear magnetic resonance; FTIR, Fourier transform infrared; HSQC, heteronuclear single quantum coherence; WAXS, wide-angle X-ray scattering; DSC, differential scanning calorimetry; TGA, thermogravimetric analysis; DMA, dynamic mechanical analysis; 3HHDA, 3-hydroxyhexaneioic acid; AA, adipic acid; HMDA, hexamethylenediamine; CH₃OH, methanol; HFIP, 1,1,1,3,3,3-hexafluoroisopropanol; TMS, tetramethyl silane; T_m, melting temperature; T_c, crystallization temperature; XRD, X-ray diffraction; χ_c, percent crystallinity; T_g, glass transition temperature; RAF, rigid amorphous fraction; MAF, mobile amorphous fraction; T₅, temperature at 5% mass loss; E', storage modulus; E'', loss modulus; ΔH_c, crystallization enthalpy.

SUPPORTIN INFORMATION

A, Molecular weight determination; B, Methods for screening results; C, Screening results for thermal analysis; D, Screening results for WAXS; E, BAN salt characterization; F, BAN heteronuclear single quantum coherence (HSQC) spectra; G, Thermogravimetric analysis plots; H, Tensile tests; I, Flexural tests; J, Moisture absorption

REFERENCES

- (1) Lipinsky, E. S. Chemicals from Biomass: Petrochemical Substitution Options. *Science* **1981**, *212* (4502), 1465–1471. https://doi.org/10.1126/science.212.4502.1465.
- (2) Levy, P. F.; Sanderson, J. E.; Kispert, R. G.; Wise, D. L. Biorefining of Biomass to Liquid Fuels and Organic Chemicals. *Enzyme Microb. Technol.* **1981**, *3* (3), 207–215. https://doi.org/10.1016/0141-0229(81)90087-9.
- (3) Clausen, E. C.; Gaddy, J. C. Organic Acids from Biomass by Continuous Fermentation. *Chem Eng Prog U. S.* **1984**, *80:12*.
- (4) McGinnis, G. D.; Wilson, W. W.; Prince, S. E.; Chen, C. C. Conversion of Biomass into Chemicals with High-Temperature Wet Oxidation. *Ind. Eng. Chem. Prod. Res. Dev.* **1983**, *22* (4), 633–636. https://doi.org/10.1021/i300012a022.
- (5) Werpy, T.; Petersen, G. *Top Value Added Chemicals from Biomass: Volume I -- Results of Screening for Potential Candidates from Sugars and Synthesis Gas*; DOE/GO-102004-1992; National Renewable Energy Lab., Golden, CO (US), 2004. https://doi.org/10.2172/15008859.
- (6) Bozell, J. J.; Petersen, G. R. Technology Development for the Production of Biobased Products from Biorefinery Carbohydrates—the US Department of Energy's "Top 10" Revisited. *Green Chem.* **2010**, *12* (4), 539–554. https://doi.org/10.1039/B922014C.
- (7) Zhang, Y. The Links between the Price of Oil and the Value of US Dollar. *Int. J. Energy Econ. Policy* **2013**, *3* (4), n/a.
- (8) Wyman, C. E. BIOMASS ETHANOL: Technical Progress, Opportunities, and Commercial Challenges. *Annu. Rev. Energy Environ.* **1999**, *24* (1), 189–226. https://doi.org/10.1146/annurev.energy.24.1.189.
- (9) Songer, D. Verdezyne Becomes Latest Victim of Liquidation, as Investors Withdraw Funding. *Bio Market Insights*, 2018.
- (10) Schill, S. Ethanol Producer Magazine The Latest News and Data About Ethanol Production http://ethanolproducer.com/articles/9872/western-biomass-up-for-sale-blue-sugars-files-bankruptcy (accessed 2020 -12 -14).
- (11) Voegele, E. Shell files bid to purchase Abengoa's cellulosic ethanol plant | Biomassmagazine.com http://biomassmagazine.com/articles/13792/shell-files-bid-to-purchase-abengoaundefineds-cellulosic-ethanol-plant (accessed 2020 -12 -14).
- (12) Dent, M. What the Oil Price Crash Means for Bioplastics https://www.idtechex.com/en/research-article/what-the-oil-price-crash-means-for-bioplastics/21301 (accessed 2020 -12 -14).
- (13) McCoy, M. Succinic acid, once a biobased chemical star, is barely being made https://cen.acs.org/business/biobased-chemicals/Succinic-acid-once-biobased-chemical/97/i12 (accessed 2020 -12 -14).

- (14) H. Shanks, B.; L. Keeling, P. Bioprivileged Molecules: Creating Value from Biomass. *Green Chem.* **2017**, *19* (14), 3177–3185. https://doi.org/10.1039/C7GC00296C.
- (15) Brownlee, H. J.; Miner, C. S. Industrial Development of Furfural. *Ind. Eng. Chem.* **1948**, *40* (2), 201–204. https://doi.org/10.1021/ie50458a005.
- (16) Peters, F. N. The Furans: Fifteen Years of Progress. *Ind. Eng. Chem.* **1936**, *28* (7), 755–759. https://doi.org/10.1021/ie50319a002.
- (17) Dalvand, K.; Rubin, J.; Gunukula, S.; Clayton Wheeler, M.; Hunt, G. Economics of Biofuels: Market Potential of Furfural and Its Derivatives. *Biomass Bioenergy* **2018**, *115*, 56–63. https://doi.org/10.1016/j.biombioe.2018.04.005.
- (18) Hernández, N.; Christopher Williams, R.; W. Cochran, E. The Battle for the "Green" Polymer. Different Approaches for Biopolymer Synthesis: Bioadvantaged vs. Bioreplacement. *Org. Biomol. Chem.* **2014**, *12* (18), 2834–2849. https://doi.org/10.1039/C3OB42339E.
- (19) Lin, F.-Y.; Hohmann, A. D.; Hernández, N.; Shen, L.; Dietrich, H.; Cochran, E. W. Self-Assembly of Poly(Styrene-Block-Acrylated Epoxidized Soybean Oil) Star-Brush-Like Block Copolymers. *Macromolecules* **2020**, *53* (18), 8095–8107. https://doi.org/10.1021/acs.macromol.0c00441.
- (20) Li, P.; Ma, S.; Dai, J.; Liu, X.; Jiang, Y.; Wang, S.; Wei, J.; Chen, J.; Zhu, J. Itaconic Acid as a Green Alternative to Acrylic Acid for Producing a Soybean Oil-Based Thermoset: Synthesis and Properties. *ACS Sustain. Chem. Eng.* **2017**, *5* (1), 1228–1236. https://doi.org/10.1021/acssuschemeng.6b02654.
- (21) Mauck, S. C.; Wang, S.; Ding, W.; Rohde, B. J.; Fortune, C. K.; Yang, G.; Ahn, S.-K.; Robertson, M. L. Biorenewable Tough Blends of Polylactide and Acrylated Epoxidized Soybean Oil Compatibilized by a Polylactide Star Polymer. *Macromolecules* **2016**, *49* (5), 1605–1615. https://doi.org/10.1021/acs.macromol.5b02613.
- (22) Bruggeman, J. P.; Bettinger, C. J.; Nijst, C. L. E.; Kohane, D. S.; Langer, R. Biodegradable Xylitol-Based Polymers. *Adv. Mater.* **2008**, *20* (10), 1922–1927. https://doi.org/10.1002/adma.200702377.
- (23) Gang, H.; Lee, D.; Choi, K.-Y.; Kim, H.-N.; Ryu, H.; Lee, D.-S.; Kim, B.-G. Development of High Performance Polyurethane Elastomers Using Vanillin-Based Green Polyol Chain Extender Originating from Lignocellulosic Biomass. *ACS Sustain. Chem. Eng.* **2017**, *5* (6), 4582–4588. https://doi.org/10.1021/acssuschemeng.6b02960.
- (24) Furtwengler, P.; Avérous, L. Renewable Polyols for Advanced Polyurethane Foams from Diverse Biomass Resources. *Polym. Chem.* **2018**, *9* (32), 4258–4287. https://doi.org/10.1039/C8PY00827B.
- (25) Lang, K.; Sánchez-Leija, R. J.; Gross, R. A.; Linhardt, R. J. Review on the Impact of Polyols on the Properties of Bio-Based Polyesters. *Polymers* **2020**, *12* (12), 2969. https://doi.org/10.3390/polym12122969.
- (26) Chen, C.; Podolsky, J. H.; Williams, R. C.; Cochran, E. W. Laboratory Investigation of Using Acrylated Epoxidized Soybean Oil (AESO) for Asphalt Modification. *Constr. Build. Mater.* **2018**, *187*, 267–279. https://doi.org/10.1016/j.conbuildmat.2018.07.204.
- (27) Half of producing shale oil wells are profitable at \$40/bbl, analyst says https://www.spglobal.com/marketintelligence/en/news-insights/latest-news-headlines/half-of-producing-shale-oil-wells-are-profitable-at-40-bbl-analyst-says-60035427 (accessed 2020 -12 -17).
- (28) Oil and Gas Activity Grows Modestly as Oil Price Jumps https://www.dallasfed.org:443/research/surveys/des/2019/1901 (accessed 2020 -12 -17).
- (29) Boulamanti, A.; Moya, J. A. Production Costs of the Chemical Industry in the EU and Other Countries: Ammonia, Methanol and Light Olefins. *Renew. Sustain. Energy Rev.* **2017**, *68*, 1205–1212. https://doi.org/10.1016/j.rser.2016.02.021.
- (30) Xie, N.-Z.; Liang, H.; Huang, R.-B.; Xu, P. Biotechnological Production of Muconic Acid: Current Status and Future Prospects. *Biotechnol. Adv.* **2014**, *32* (3), 615–622. https://doi.org/10.1016/j.biotechadv.2014.04.001.

- (31) Vardon, D. R.; Franden, M. A.; Johnson, C. W.; Karp, E. M.; Guarnieri, M. T.; Linger, J. G.; Salm, M. J.; Strathmann, T. J.; Beckham, G. T. Adipic Acid Production from Lignin. *Energy Environ. Sci.* **2015**, *8* (2), 617–628. https://doi.org/10.1039/C4EE03230F.
- (32) Bentley, G. J.; Narayanan, N.; Jha, R. K.; Salvachúa, D.; Elmore, J. R.; Peabody, G. L.; Black, B. A.; Ramirez, K.; De Capite, A.; Michener, W. E.; Werner, A. Z.; Klingeman, D. M.; Schindel, H. S.; Nelson, R.; Foust, L.; Guss, A. M.; Dale, T.; Johnson, C. W.; Beckham, G. T. Engineering Glucose Metabolism for Enhanced Muconic Acid Production in Pseudomonas Putida KT2440. *Metab. Eng.* **2020**, *59*, 64–75. https://doi.org/10.1016/j.ymben.2020.01.001.
- (33) Suastegui, M.; Matthiesen, J. E.; Carraher, J. M.; Hernandez, N.; Rodriguez Quiroz, N.; Okerlund, A.; Cochran, E. W.; Shao, Z.; Tessonnier, J.-P. Combining Metabolic Engineering and Electrocatalysis: Application to the Production of Polyamides from Sugar. *Angew. Chem. Int. Ed.* **2016**, *55* (7), 2368–2373. https://doi.org/10.1002/anie.201509653.
- (34) Suástegui, M.; Yu Ng, C.; Chowdhury, A.; Sun, W.; Cao, M.; House, E.; Maranas, C. D.; Shao, Z. Multilevel Engineering of the Upstream Module of Aromatic Amino Acid Biosynthesis in Saccharomyces Cerevisiae for High Production of Polymer and Drug Precursors. *Metab. Eng.* **2017**, *42*, 134–144. https://doi.org/10.1016/j.ymben.2017.06.008.
- (35) Beerthuis, R.; Rothenberg, G.; Shiju, N. R. Catalytic Routes towards Acrylic Acid, Adipic Acid and ε-Caprolactam Starting from Biorenewables. *Green Chem.* **2015**, *17* (3), 1341–1361. https://doi.org/10.1039/C4GC02076F.
- (36) Matthiesen, J. E.; Carraher, J. M.; Vasiliu, M.; Dixon, D. A.; Tessonnier, J.-P. Electrochemical Conversion of Muconic Acid to Biobased Diacid Monomers. ACS Sustain. Chem. Eng. 2016, 4 (6), 3575–3585. https://doi.org/10.1021/acssuschemeng.6b00679.
- (37) Matthiesen, J. E.; Suástegui, M.; Wu, Y.; Viswanathan, M.; Qu, Y.; Cao, M.; Rodriguez-Quiroz, N.; Okerlund, A.; Kraus, G.; Raman, D. R.; Shao, Z.; Tessonnier, J.-P. Electrochemical Conversion of Biologically Produced Muconic Acid: Key Considerations for Scale-Up and Corresponding Technoeconomic Analysis. *ACS Sustain. Chem. Eng.* **2016**, *4* (12), 7098–7109. https://doi.org/10.1021/acssuschemeng.6b01981.
- (38) Fox, T. G.; Loshaek, S. Influence of molecular weight and degree of crosslinking on the specific volume and glass temperature of polymers. *J. Polym. Sci.* **1955**, *15* (80), 371–390. https://doi.org/10.1002/pol.1955.120158006.
- (39) Nunes, R. W.; Martin, J. R.; Johnson, J. F. Influence of Molecular Weight and Molecular Weight Distribution on Mechanical Properties of Polymers. *Polym. Eng. Sci.* **1982**, *22* (4), 205–228. https://doi.org/10.1002/pen.760220402.
- (40) Mohd-Adnan, A.-F.; Nishida, H.; Shirai, Y. Evaluation of Kinetics Parameters for Poly(I-Lactic Acid) Hydrolysis under High-Pressure Steam. *Polym. Degrad. Stab.* 2008, 93 (6), 1053–1058. https://doi.org/10.1016/j.polymdegradstab.2008.03.022.
- (41) Höfle, G.; Steglich, W.; Vorbrüggen, H. 4-Dialkylaminopyridines as Highly Active Acylation Catalysts. [New Synthetic Method (25)]. *Angew. Chem. Int. Ed. Engl.* **1978**, *17* (8), 569–583. https://doi.org/10.1002/anie.197805691.
- (42) Orita, A.; Tanahashi, C.; Kakuda, A.; Otera, J. Highly Powerful and Practical Acylation of Alcohols with Acid Anhydride Catalyzed by Bi(OTf)3. *J. Org. Chem.* **2001**, *66* (26), 8926–8934. https://doi.org/10.1021/jo0107453.
- (43) Procopiou, P. A.; Baugh, S. P. D.; Flack, S. S.; Inglis, G. G. A. An Extremely Powerful Acylation Reaction of Alcohols with Acid Anhydrides Catalyzed by Trimethylsilyl Trifluoromethanesulfonate. *J. Org. Chem.* **1998**, 63 (7), 2342–2347. https://doi.org/10.1021/jo980011z.
- (44) Ramesh, C.; Keller, A.; Eltink, S. J. E. A. Studies on the Crystallization and Melting of Nylon-6,6: 1. The Dependence of the Brill Transition on the Crystallization Temperature. *Polymer* **1994**, *35* (12), 2483–2487. https://doi.org/10.1016/0032-3861(94)90367-0.

- (45) Feldman, A. Y.; Wachtel, E.; Vaughan, G. B. M.; Weinberg, A.; Marom, G. The Brill Transition in Transcrystalline Nylon-66. *Macromolecules* **2006**, *39* (13), 4455–4459. https://doi.org/10.1021/ma060487h.
- (46) Feldman, A. Y.; Fernanda Gonzalez, M.; Wachtel, E.; Moret, M. P.; Marom, G. Transcrystallinity in Aramid and Carbon Fiber Reinforced Nylon 66: Determining the Lamellar Orientation by Synchrotron X-Ray Micro Diffraction. *Polymer* **2004**, *45* (21), 7239–7245. https://doi.org/10.1016/j.polymer.2004.08.027.
- (47) Starkweather, H. W.; Jones, G. A. Crystalline Transitions in Powders of Nylon 66 Crystallized from Solution. *J. Polym. Sci. Polym. Phys. Ed.* **1981**, *19* (3), 467–477. https://doi.org/10.1002/pol.1981.180190307.
- (48) Murthy, N. S.; Curran, S. A.; Aharoni, S. M.; Minor, H. Premelting Crystalline Relaxations and Phase Transitions in Nylon 6 and 6,6. *Macromolecules* **1991**, *24* (11), 3215–3220. https://doi.org/10.1021/ma00011a027.
- (49) Mandelkern, L. The Relation between Structure and Properties of Crystalline Polymers. *Polym. J.* **1985**, *17* (1), 337–350. https://doi.org/10.1295/polymj.17.337.
- (50) Flory, P. J. Thermodynamics of Crystallization in High Polymers II. Simplified Derivation of Melting-Point Relationships. *J. Chem. Phys.* **1947**, *15* (9), 684–684. https://doi.org/10.1063/1.1746627.
- (51) Flory, P. J.; Mandelkern, L.; Hall, H. K. Crystallization in High Polymers. VII. Heat of Fusion of Poly-(N,N'-Sebacoylpiperazine) and Its Interaction with Diluents1. *J. Am. Chem. Soc.* **1951**, *73* (6), 2532–2538. https://doi.org/10.1021/ja01150a035.
- (52) Evans, R. D.; Mighton, H. R.; Flory, P. J. Crystallization in High Polymers. V. Dependence of Melting Temperatures of Polyesters and Polyamides on Composition and Molecular Weight1,2. *J. Am. Chem. Soc.* **1950**, *72* (5), 2018–2028. https://doi.org/10.1021/ja01161a040.
- (53) Flory, P. J. Theory of Crystallization in Copolymers. *Trans. Faraday Soc.* **1955**, *51* (0), 848–857. https://doi.org/10.1039/TF9555100848.
- (54) Di Lorenzo, M. L.; Androsch, R.; Stolte, I. Tailoring the Rigid Amorphous Fraction of Isotactic Polybutene-1 by Ethylene Chain Defects. *Polymer* **2014**, *55* (23), 6132–6139. https://doi.org/10.1016/j.polymer.2014.09.040.
- (55) Murthy, N. S.; Wang, Z.-G.; Hsiao, B. S. Interactions between Crystalline and Amorphous Domains in Semicrystalline Polymers: Small-Angle X-Ray Scattering Studies of the Brill Transition in Nylon 6,6. *Macromolecules* **1999**, *32* (17), 5594–5599. https://doi.org/10.1021/ma990475e.
- (56) Yang, X.; Tan, S.; Li, G.; Zhou, E. Dependence of the Brill Transition on the Crystal Size of Nylon 10 10. *Macromolecules* **2001**, *34* (17), 5936–5942. https://doi.org/10.1021/ma002091q.
- (57) Wolanov, Y.; Feldman, A. Y.; Harel, H.; Marom, G. Amorphous and Crystalline Phase Interaction during the Brill Transition in Nylon 66. *Express Polym. Lett.* **2009**, *3* (7), 452–457. https://doi.org/10.3144/expresspolymlett.2009.55.
- (58) Flory, P. J.; Yoon, D. Y. Molecular Morphology in Semicrystalline Polymers. *Nature* **1978**, *272* (5650), 226–229. https://doi.org/10.1038/272226a0.
- (59) Lorenzo, M. L. D.; Righetti, M. C. Crystallization-Induced Formation of Rigid Amorphous Fraction. *Polym. Cryst.* **2018**, *1* (2), e10023. https://doi.org/10.1002/pcr2.10023.
- (60) Di Lorenzo, M. L.; Gazzano, M.; Righetti, M. C. The Role of the Rigid Amorphous Fraction on Cold Crystallization of Poly(3-Hydroxybutyrate). *Macromolecules* **2012**, *45* (14), 5684–5691. https://doi.org/10.1021/ma3010907.
- (61) Domszy, R. C.; Alamo, R.; Mathieu, P. J. M.; Mandelkern, L. The Structure of Copolymer Crystals Formed from Dilute Solution and in Bulk. *J. Polym. Sci. Polym. Phys. Ed.* **1984**, *22* (10), 1727–1744. https://doi.org/10.1002/pol.1984.180221003.
- (62) Stolte, I.; Androsch, R.; Di Lorenzo, M. L. Spherulite Growth Rate and Fold Surface Free Energy of the Form II Mesophase in Isotactic Polybutene-1 and Random Butene-1/Ethylene Copolymers. *Colloid Polym. Sci.* **2014**, *292* (6), 1479–1485. https://doi.org/10.1007/s00396-014-3221-0.

- (63) Kolstad, J. J. Crystallization Kinetics of Poly(L-Lactide-Co-Meso-Lactide). *J. Appl. Polym. Sci.* **1996**, *62* (7), 1079–1091. https://doi.org/10.1002/(SICI)1097-4628(19961114)62:7<1079::AID-APP14>3.0.CO;2-1.
- (64) Lin, T.; Cogen, J.; Lyon, R. Correlations between Microscale Combustion Calorimetry and Conventional Flammability Tests for Flame Retardant Wire and Cable Compounds. 56th IWCS Conf. Proc. Int. Wire Cable Symp. Inc IWCS 2007 2007.
- (65) Holland, B. J.; Hay, J. N. Thermal Degradation of Nylon Polymers. *Polym. Int.* **2000**, *49* (9), 943–948. https://doi.org/10.1002/1097-0126(200009)49:9<943::AID-PI400>3.0.CO;2-5.
- (66) S. Lima, M.; F. Costa, C. S. M.; J. Coelho, J. F.; C. Fonseca, A.; C. Serra, A. A Simple Strategy toward the Substitution of Styrene by Sobrerol-Based Monomers in Unsaturated Polyester Resins. *Green Chem.* 2018, 20 (21), 4880–4890. https://doi.org/10.1039/C8GC01214H.
- (67) Taniguchi, A.; Cakmak, M. The Suppression of Strain Induced Crystallization in PET through Sub Micron TiO2 Particle Incorporation. *Polymer* 2004, 45 (19), 6647–6654. https://doi.org/10.1016/j.polymer.2004.06.056.
- (68) Huang, X.; Nakagawa, S.; Houjou, H.; Yoshie, N. Insights into the Role of Hydrogen Bonds on the Mechanical Properties of Polymer Networks. *Macromolecules* 2021, 54 (9), 4070–4080. https://doi.org/10.1021/acs.macromol.1c00120.
- (69) The Definitive Guide to ISO 178; https://www.instron.us/en-US/Testing Solutions/By Test Type/Flexure/The Definitive Guide to ISO 178 Flexure Testing for Plastics (accessed 2020 -12 -21).
- (70) Flexural Strength Testing of Plastics http://www.matweb.com/reference/flexuralstrength.aspx (accessed 2020 -12 -21).
- (71) Cousin, T.; Galy, J.; Rousseau, A.; Dupuy, J. Synthesis and Properties of Polyamides from 2,5-Furandicarboxylic Acid. *J. Appl. Polym. Sci.* **2018**, *135* (8), 45901. https://doi.org/10.1002/app.45901.
- (72) Yang, T.; Mutua, F. N.; Gao, Y.; Li, S.; Dong, H.; Zhu, B.; He, Y. Synthesis and Characterization of Poly (1,6-Hexamethylene Oxamide-Co-m-Xylene Oxamide) Copolymers. *Polym. Adv. Technol.* **2018**, *29* (12), 2943–2951. https://doi.org/10.1002/pat.4414.
- (73) Kohan, M. I. *Nylon Plastics Handbook*; Hanser Publishers; Distributed in the USA and in Canada by Hanser/Gardner Publications: Munich; New York; Cincinnati, 1995.
- (74) Jia, N.; Kagan, V. A. Mechanical Performance of Polyamides with Influence of Moisture and Temperature Accurate Evaluation and Better Understanding. In *Plastics Failure Analysis and Prevention*; Elsevier, 2001; pp 95–104. https://doi.org/10.1016/B978-188420792-1.50014-7.
- (75) Zytel® 101 NC010 | DuPont https://dupont.materialdatacenter.com/en/products/datasheet/SI/Zytel%C2%AE%20101%20NC010 (accessed 2021 -03 -03).
- (76) Bettenhausen, C. Cargill and Helm form joint venture to build \$300 million biobased 1,4-butanediol plant in Iowa https://cen.acs.org/materials/polymers/Cargill-Helm-form-joint-venture/99/i22 (accessed 2021 07 -06).
- (77) Katti, S. S.; Schultz, M. The Microstructure of Injection-Molded Semicrystalline Polymers: A Review. *Polym. Eng. Sci.* **1982**, *22* (16), 1001–1017. https://doi.org/10.1002/pen.760221602.
- (78) Starkweather, H. W.; Moore, G. E.; Hansen, J. E.; Roder, T. M.; Brooks, R. E. Effect of Crystallinity on the Properties of Nylons. *J. Polym. Sci.* **1956**, *21* (98), 189–204. https://doi.org/10.1002/pol.1956.120219803.
- (79) Moran, C. S.; Barthelon, A.; Pearsall, A.; Mittal, V.; Dorgan, J. R. Biorenewable Blends of Polyamide-4,10 and Polyamide-6,10. *J. Appl. Polym. Sci.* **2016**, *133* (45). https://doi.org/10.1002/app.43626.